V64

Modern Interferometry

Alexander Sonntag
alexander.sonntag@tu-dortmund.de

Malte Zimmermann
malte.zimmermann@tu-dortmund.de

Durchführung: 10.11.2025 Abgabe: 18.11.2025

TU Dortmund – Fakultät Physik

Contents

1 Objective **3**

2 Theory **3**
- 2.1 Polarization . . . 3
- 2.2 Coherence . . . 4
- 2.3 Interference . . . 5
- 2.4 Interferometers . . . 6
  - 2.4.1 The Sagnac Interferometer . . . 6
  - 2.4.2 Operation of a PBSC (Polarizing Beam Splitter Cube) . . . 9
  - 2.4.3 Maximum and Minimum Intensity at the Detector . . . 10
  - 2.4.4 Contrast/Visibility of an Interferometer . . . 11
  - 2.4.5 Determination of Refractive Indices . . . 11

3 Experimental Setup and Procedure **12**
- 3.1 The Experimental Setup . . . 12
- 3.2 Experimental Procedure . . . 13
  - 3.2.1 Alignment . . . 13
  - 3.2.2 Measurements . . . 14

4 Analysis **14**
- 4.1 Polarization dependence of the contrast . . . 14
- 4.2 Refractive index of glass . . . 16
- 4.3 Refractive index of air . . . 16

5 Discussion **18**

6 Appendix **19**

References **22**

1 Objective

The objective of this experiment is to understand the operation of a Sagnac interferometer. In this context, the refractive index of glass and air is to be experimentally determined using interferometry.

2 Theory

This section discusses the theoretical foundations of interferometry. Among other topics, coherence and polarization are described. These are the essential building blocks of interferometry.

2.1 Polarization

Light, described as an electromagnetic wave, can exhibit four different forms of polarization. The magnetic field component is always perpendicular to the electric one. In the following, only the electric field component $\vec{E}$ is considered for simplification. The four polarization forms are:

(1) Linearly polarized: The electric field component oscillates in a fixed plane (see fig. 1).

(2) Circularly polarized: A distinction is made here between right-circular (RCP) and left-circular (LCP). The electric field component rotates circularly in the plane perpendicular to the wave vector $\vec{k}$ (see fig. 1).

(3) Elliptically polarized: The electric field component rotates elliptically in the plane perpendicular to $\vec{k}$ (see fig. 1).

(4) Unpolarized light: Here, there is no preferred orientation of the electric field component. The polarization changes statistically millions of times per second [1].

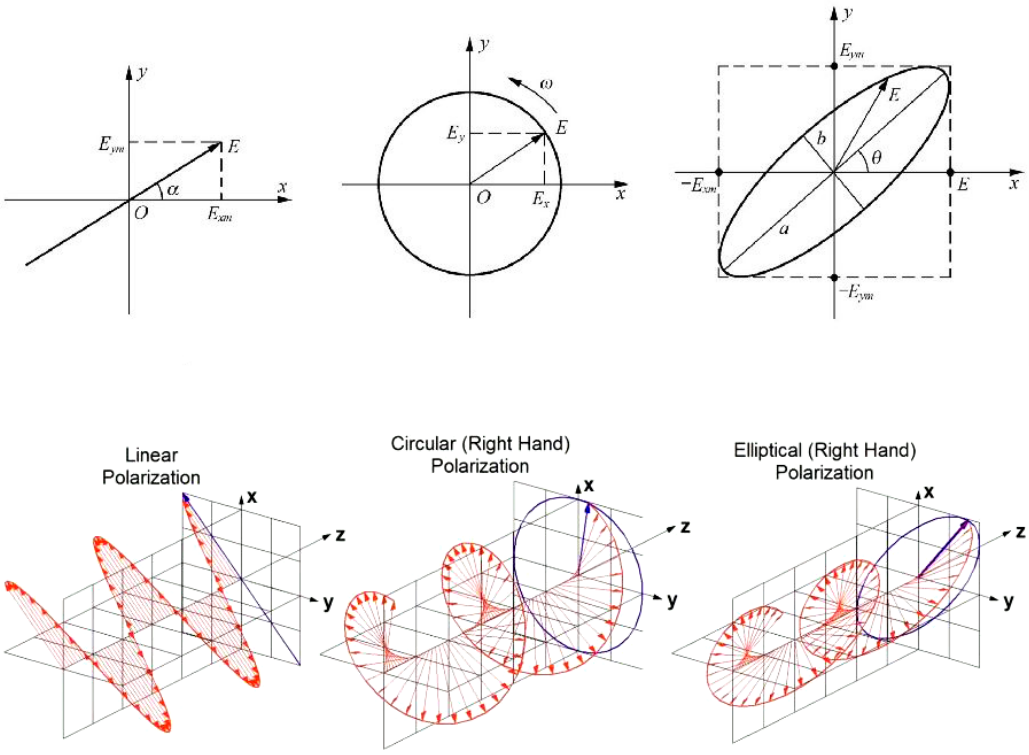

Figure 1: Schematic representation of linear, circular, and elliptical polarization [2]. The fixed reference plane is the x–y plane for all three (reference plane = fixed plane in which the orientation and motion of the electric field vector $\vec{E}$ are described, while the wave vector $\vec{k}$ is perpendicular to it). The wave vector $\vec{k}$ and the z-axis point in the same direction. Consequently, the wave vector $\vec{k}$ is oriented normal to the x–y plane.

2.2 Coherence

Coherence is a property of wave trains in which the phase is preserved (i.e., the phase is constant). If a wave always oscillates with the same phase position, the sequence of wave crests and troughs is stable. Consequently, if two waves superpose, $\vec{E}_1$ and $\vec{E}_2$ (representing the electric field vectors), and maintain a constant phase difference over the observation period, observable interference effects arise. If the phase difference fluctuates significantly, the interference term averages out (see formula (1) and also section 2.3) [3], [1]. This phase stability is the core of coherence. A distinction is made between temporal and spatial coherence. T Temporal coherence describes the stability of the phase of a wave at a given point in space over time. It indicates how long a wave can maintain a predictable phase relationship, which is essential for producing sustained interference patterns. Spatial coherence refers to the correlation of the phase between different points in space at the same moment in time, determining how well-separated points can exhibit interference effects. In the ideal case of perfect temporal and spatial coherence, the crests

and troughs of the wave form a fully predictable and stable pattern relative to each other, while the wave continues to propagate and the electric field continues to oscillate in space and time. This predictable phase relationship is the essence of coherence, enabling high-contrast interference phenomen [1]. The degree of coherence is described by the absolute value of the complex coherence function

$$|\gamma_{12}(\tau)| = \left| \frac{\langle E_1(t+\tau) E_2^*(t) \rangle_T}{\sqrt{\langle |E_1|^2 \rangle \langle |E_2|^2 \rangle}} \right|, \quad [1] \tag{1}$$

the degree of coherence. The quantities E_1 and E_2 represent the complex electric fields at the spatial points S_1 and S_2, respectively. These fields describe the optical disturbances at the two points, including both their amplitudes and phases. The variable t denotes the time of observation, while τ represents the temporal delay between the two fields. The expression involving $E_1(t+\tau)$ and $E_2(t)$ quantifies the degree of phase coherence between the two fields, indicating how well their relative phases are preserved when one of the fields is shifted in time by τ. $\langle ... \rangle_T$ denotes the time average. It holds that:

$$|\gamma_{12}(\tau)| = \begin{cases} 1, & \text{coherent limiting case} \\ 0, & \text{incoherent limiting case} \\ 0 < |\gamma_{12}(\tau)| < 1, & \text{partially coherent case} \end{cases}$$

2.3 Interference

When two or more wave trains overlap and this leads to cancellation (partial or complete) or amplification (partial or complete) due to phase shifts between them, this is referred to as interference. Expressed in formulas, the resulting light intensity is

$$I = I_1 + I_2 + 2\sqrt{I_1 I_2}\, |\gamma_{12}(\tau)| \cos(\Phi_{12}(\tau)), \quad [1] \tag{2}$$

with $|\gamma_{12}(\tau)|$ the degree of coherence, I_i the intensities of the individual waves, τ temporal offset between the electric fields, and $\Phi_{12}(\tau)$ the phase shift of the (complex) coherence function $\gamma_{12}(\tau)$ between the fields E_1 and E_2. It holds that $\Phi_{12}(\tau) = \alpha_{12} - \varphi$ [1], where α_{12} is the statistical field phase (arising from the stationary fluctuations of the electric fields themselves) and φ is the classical phase difference, described by

$$\varphi = \frac{2\pi}{\lambda}(r_2 - r_1),$$

with the optical path length $r_2 - r_1$ and the wavelength λ. The cos term in formula (2) determines constructive or destructive interference:

$$\cos(\Phi_{12}(\tau)) = \begin{cases} +1, & \text{for } \Phi_{12}(\tau) = 2\pi n,\ n \in \mathbb{N}_0 \quad \text{constructive interference} \\ -1, & \text{for } \Phi_{12}(\tau) = (2n+1)\pi,\ n \in \mathbb{N}_0 \quad \text{destructive interference} \end{cases}$$

Furthermore, it holds that

$$I = \varepsilon_0 \frac{c}{n} \langle \vec{E}^2 \rangle_T \propto \langle \vec{E}^2 \rangle_T,$$

with $\langle \vec{E}^2 \rangle_T$ the time-averaged value of the square of the magnitude of the electric field vector $\vec{E}^2$ over a period T. In addition, ε_0 stands for the vacuum permittivity, c for the speed of light in vacuum, and n for the refractive index of the medium in which the wave propagates (for vacuum: $n = 1$). To observe interference phenomena, the polarization directions must be parallel or partially overlapping. With perpendicular polarization, no interference is observable. Expressed in a formula with the polarization unit vectors $\hat{e}_i$, $I = I_1 + I_2 + 2\sqrt{I_1 I_2}\,|\gamma_{12}(\tau)|\cos(\Phi_{12}) \cdot (\hat{e}_1 \cdot \hat{e}_2)$ [1].

2.4 Interferometers

Interferometers are used to perform interferometric measurements. Three well-known ones are the Michelson, Mach-Zehnder, and Sagnac interferometers. The latter has the highest stability against external disturbances and is used in this experiment [1].

2.4.1 The Sagnac Interferometer

Broadly speaking, the Sagnac interferometer consists of three mirrors and a beam splitter; see Fig. 2. The beam splitter divides the incoming beam into two identical but counter-propagating partial beams. The counter-propagating beams then meet again at the beam splitter and are directed to the detector.

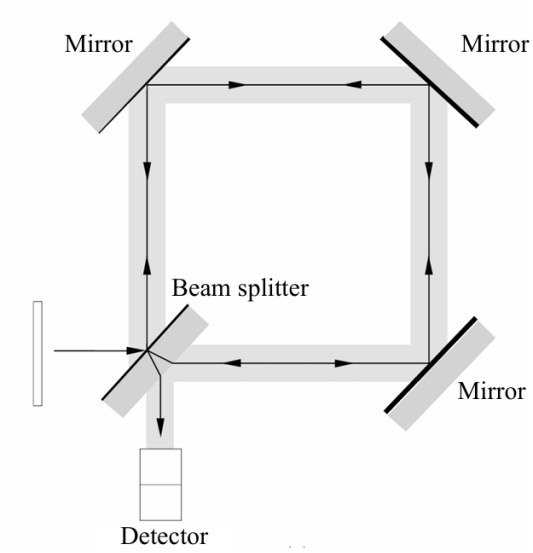

Figure 2: Schematic representation of the Sagnac interferometer [1].

To generate a phase shift, two methods can be chosen:

(1) Rotation method: In this method, the entire Sagnac interferometer is rotated around its symmetry axis with the angular velocity (rotation rate) Ω, see Fig. 3. The beam splitter divides the laser beam into two counter-propagating beams: one clockwise (CW) and one counterclockwise (CCW). Due to the spatial positions of

the reflecting elements (here, the mirrors) changing as a result of the rotation, the light does not change its speed. For the beam propagating in the CW direction, the next reflection point shifts toward the beam during the light's travel time. The beam therefore reaches the mirror only after covering a longer distance, even though its speed relative to the local space always remains c (speed of light). For the beam in the CCW direction, the next reflection point shifts in the opposite direction during the light's travel time, which shortens the actual distance the beam has to travel [4]. In Fig. 4, the laser beam enters the beam splitter at point A, where it is split into two counter-propagating beams. At point A', the two beams are recombined. Due to the rotation of the entire system, this point is no longer identical to the original point A; thus, $A' \neq A$. Expressed in formulas

$$L = 2\pi R,$$

where R is the radius of the circular disk on which the interferometer is located and L the path length.

$$\text{If } \Omega = 0: \quad c\,\Delta t_1 = \Delta t_2 = L = 2\pi R,$$

$$\text{If } \Omega \neq 0: \quad \begin{cases} c\,\Delta t_1 = 2\pi R + R\,\Omega\,\Delta t_1, & \text{CW case,} \\ c\,\Delta t_2 = 2\pi R - R\,\Omega\,\Delta t_2, & \text{CCW case,} \end{cases}$$

with Δt_1 and Δt_2 the light travel time and c the speed of light. For the rotated case, we thus obtain

$$\Delta t_{12} = \Delta t_1 - \Delta t_2 = \frac{4\pi R^2 \Omega}{c^2 - R^2\Omega^2} \approx \frac{4\pi R^2}{c^2}\Omega.$$

The formula can be expressed for any closed optical path as

$$\Delta t_{12} = 4\frac{\vec{\Omega}\vec{S}}{c^2},$$

with $\vec{S}$, the vector that is perpendicular to the area S enclosed by the optical path. The phase shift between the two waves is thus given by

$$\Phi_{12} = \omega \Delta t_{12} = \frac{4\omega}{c^2}(\vec{\Omega} \cdot \vec{S}),$$

with the laser frequency ω [5].

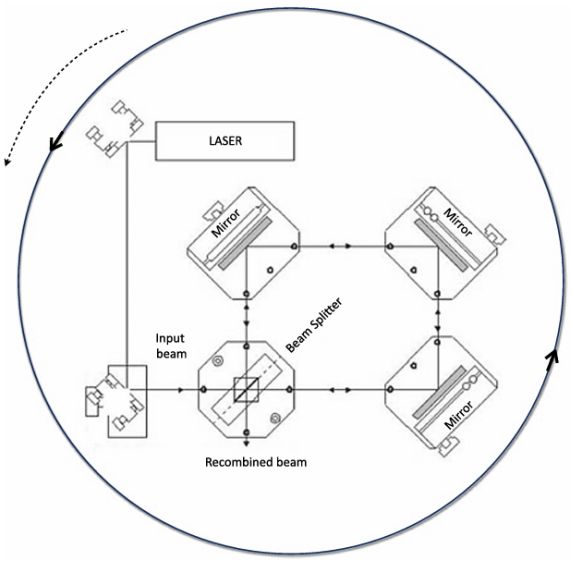

Figure 3: Rotational configuration of the Sagnac interferometer [5].

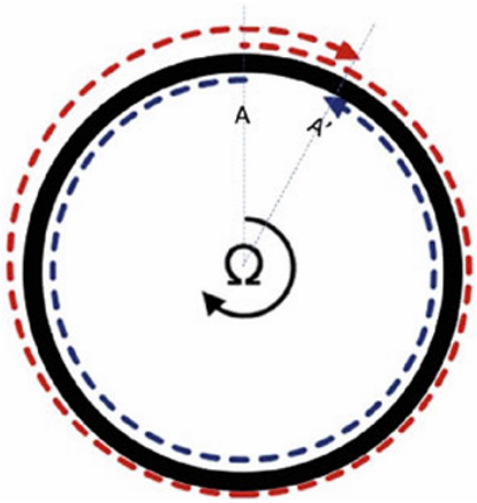

Figure 4: Schematic of the operating principle of a rotating Sagnac interferomete [5].
Both counter-propagating beams enter the interferometer at point A and recombine at point A' as a result of the rotation of the system.

(2) Rotation holder method: The second method employed in this experiment involves inserting a rotation holder into both beam paths. The beams are first separated into two parallel paths, after which the rotation holder is placed into both. The holder contains two glass plates with a refractive index of n (see Figure 5). By rotating this mount, the optical path length L_{opt} of the beams relative to each other changes, leading to a relative phase shift

$$\Phi_{12} = \frac{2\pi}{\lambda} L_{\text{opt}} = \frac{2\pi}{\lambda} (n\, L_{\text{geo.}})$$

[6]. Here, n denotes the refractive index of the glass, $L_{\text{geo.}}$ its geometric thickness, and λ the wavelength of the light.

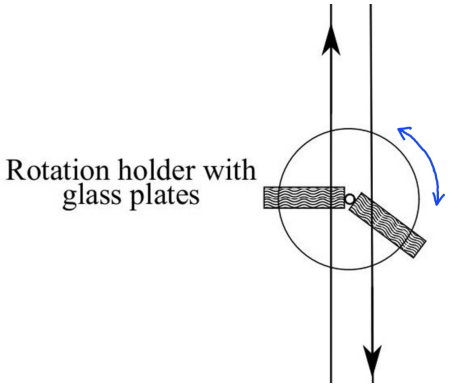

Figure 5: Rotation holder with glass plates, inserted into two parallel, counter-propagating laser beams.
By rotating the holder, the optical path length is altered, thereby producing a phase shift between the two parallel beams.

2.4.2 Operation of a PBSC (Polarizing Beam Splitter Cube)

A PBSC is installed in the setup of the Sagnac interferometer. This special beam splitter separates an incident beam into two partial beams depending on their polarization: s-polarization (perpendicular to the plane of incidence) and p-polarization (parallel to the plane of incidence). The incident beam contains both s- and p-polarized components. When it strikes the PBSC, the s-polarized component is reflected while the p-polarized component is transmitted (see Fig. 6). To ensure that the two resulting partial beams have equal intensity, the PBSC must be oriented such that the incident beam hits its surface at an angle of 45° relative to the surface normal.

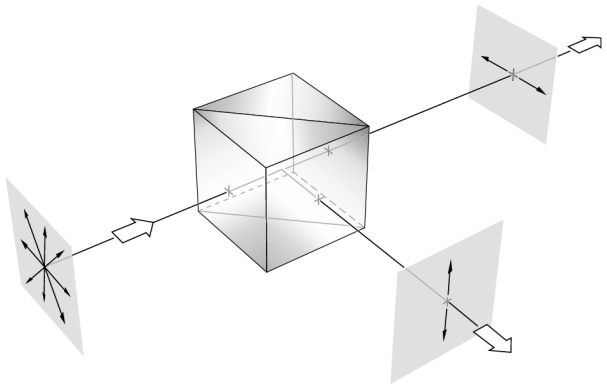

Figure 6: Schematic representation of the operation of a PBSC [1].

This orientation balances the intensities of the reflected and transmitted beams, making them equally bright. At the same time, the polarization separation ensures that the beams are orthogonally polarized and clearly separated. In this way, the PBSC produces two beams that are both equally bright and cleanly polarized, which is crucial for the proper operation of the Sagnac interferometer [1].

2.4.3 Maximum and Minimum Intensity at the Detector

The interference patterns generated by the interferometer are detected by a diode. In general, the intensity at the diode is

$$I \propto \left\langle \left| E_1 \cos(\omega t) + E_2 \cos(\omega t + \Phi_{12}) \right|^2 \right\rangle, \quad [6] \tag{3}$$

with E_i the electric field components of the two output beams of the interferometer and $\langle \ ... \ \rangle$ the time average. The following ansatz is chosen for the electric field components:

$$E_1 = E_0 \cos(\phi)$$
$$E_2 = E_0 \sin(\phi).$$

ϕ is the polarization angle of the electric field, which determines how the total amplitude E_0 is projected onto the two orthogonal components E_1 and E_2. Here, $\phi = 0$ corresponds to complete polarization along E_1, and $\phi = \pi/2$ corresponds to complete polarization along E_2.
Inserting into equation (3) yields

$$I \propto E_0^2 \left\langle \left(\left| \cos^2(\phi) \cos^2(\omega t) + 2 \cos(\phi) \cos(\omega t) \sin(\phi) \cos(\omega t + \Phi_{12}) + sin^2(\phi) \cos(\omega t + \Phi_{12}) \right) \right| \right\rangle. \tag{4}$$

Using the conditions

(I) **Maxima:** $\Phi_{12} = 2\pi n, \quad n \in \mathbb{N}_0$

(II) **Minima:** $\Phi_{12} = (2n+1)\pi, \quad n \in \mathbb{N}_0$

equation (4) simplifies for the maximum intensity to

$$\begin{aligned}
I_{\max} &\propto E_0^2 \left\langle \left| \cos^2(\omega t)(\cos^2\phi + \sin^2\phi) + 2\cos\phi\, \cos^2(\omega t)\sin\phi \right| \right\rangle \\
&\propto E_0^2 \left\langle \left| \cos^2(\omega t)(1 + 2\cos\phi\, \sin\phi) \right| \right\rangle \\
&\propto E_0^2 \left\langle \left| \cos^2(\omega t)(1 + \sin(2\phi)) \right| \right\rangle \\
&\propto E_0^2 \underbrace{\langle \cos^2(\omega t) \rangle}_{=\frac{1}{2}} (1 + \sin(2\phi)) \\
&\propto \underbrace{\frac{1}{2} E_0^2}_{\propto I_{\text{Laser}}} (1 + \sin(2\phi)) \\
&\propto I_{\text{Laser}}(1 + \sin(2\phi)).
\end{aligned}$$

Equivalently for $I_{\min}$. Accordingly, the maximum and minimum intensity at the detector are:

$$I_{\max} \propto I_{\text{Laser}}(1 + \sin(2\phi)) \tag{5}$$
$$I_{\min} \propto I_{\text{Laser}}(1 - \sin(2\phi)) \tag{6}$$

2.4.4 Contrast/Visibility of an Interferometer

The contrast or visibility of an interferometer is defined as

$$V = \left| \frac{I_{\max} - I_{\min}}{I_{\max} + I_{\min}} \right| \quad [1] \tag{7}$$

with $I_{\max}$ the intensity of a maximum in the interference pattern and $I_{\min}$ the minimum in the pattern.

$$V = \begin{cases} 1, & \text{perfect contrast, } I_{\min} = 0, \\ 0 < V < 1, & \text{reduced contrast, the interference pattern is visible,} \\ 0, & \text{no contrast, only uniform light, } I_{\max} = I_{\min}. \end{cases} \tag{8}$$

Using (5) and (6), the relationship between visibility/contrast V and the polarization angle ϕ is

$$V = \left| \frac{I_{\max} - I_{\min}}{I_{\max} + I_{\min}} \right| = |2\sin(\phi)\cos(\phi)| = |\sin(2\phi)|\,. \tag{9}$$

2.4.5 Determination of Refractive Indices

Using the interferometer, refractive indices n of solids as well as gases can be determined. For this, the number of intensity maxima M in the interference pattern is measured. This yields the relation to the phase shift through the medium Φ_{12}

$$M = \frac{\Phi_{12}}{2\pi}. \quad [6] \tag{10}$$

1. Determination of the refractive index of glass:
   For determining the refractive index of glass, the following approximation for the phase shift can be assumed, depending on the rotation angle Θ of the glass plates used:
   $$\Phi_{12}(\Theta) = \frac{2\pi}{\lambda_{\text{vac}}} \mathrm{d} \left(\frac{(n-1)}{2n} \Theta^2 + \mathcal{O}(\Theta^4) \right) \quad [6] \tag{11}$$
   Here, λ_{vac} denotes the light wavelength in vacuum, d the thickness of the glass plate, and n the refractive index. If the glass plate already has an initial rotation angle Θ_0, formula (12) is adjusted to
   $$\Phi_{12}(\Theta) = \frac{2\pi}{\lambda_{\text{vac}}} \mathrm{d} \frac{(n-1)}{2n} ((\Theta + \Theta_0)^2 - (\Theta - \Theta_0)^2) \tag{12}$$

2. Determination of the refractive index of gases:
   To experimentally determine the refractive index of gases, the relation of the phase shift Φ_{12} to the geometric length L
   $$\Phi_{12} = \frac{2\pi}{\lambda_{\text{vac}}} (n-1) L \tag{13}$$
   and (10), which provides a connection between the phase and the measured intensity maxima, are used. At the same time, the Lorentz-Lorenz law also applies
   $$\frac{n^2 - 1}{n^2 + 2} = \mathrm{A} \frac{p}{\mathrm{R}\, T} \quad [7], \tag{14}$$
   with the universal gas constant R, the molar refractivity A, as well as the measured pressure p and temperature T. For gases at low pressures, this law can be further simplified to
   $$(n-1) = \frac{3}{2} \mathrm{A} \frac{p}{\mathrm{R}\, T} \tag{15}$$
   which provides a connection between the refractive index n and the measured pressure p, as well as the ambient temperature T.

3 Experimental Setup and Procedure

This section outlines the experimental setup and briefly describes the procedure.

3.1 The Experimental Setup

The setup of the Sagnac interferometer after alignment is shown schematically in Fig. 7. It consists of a HeNe laser, two mirrors for coupling the beam into the interferometer, three additional mirrors Ma, Mb, and Mc, as well as two PBSCs and two diode detectors. Additionally, a rotatable glass plate arrangement is placed in one of the beam paths, and a polarizer is located in the input beam.

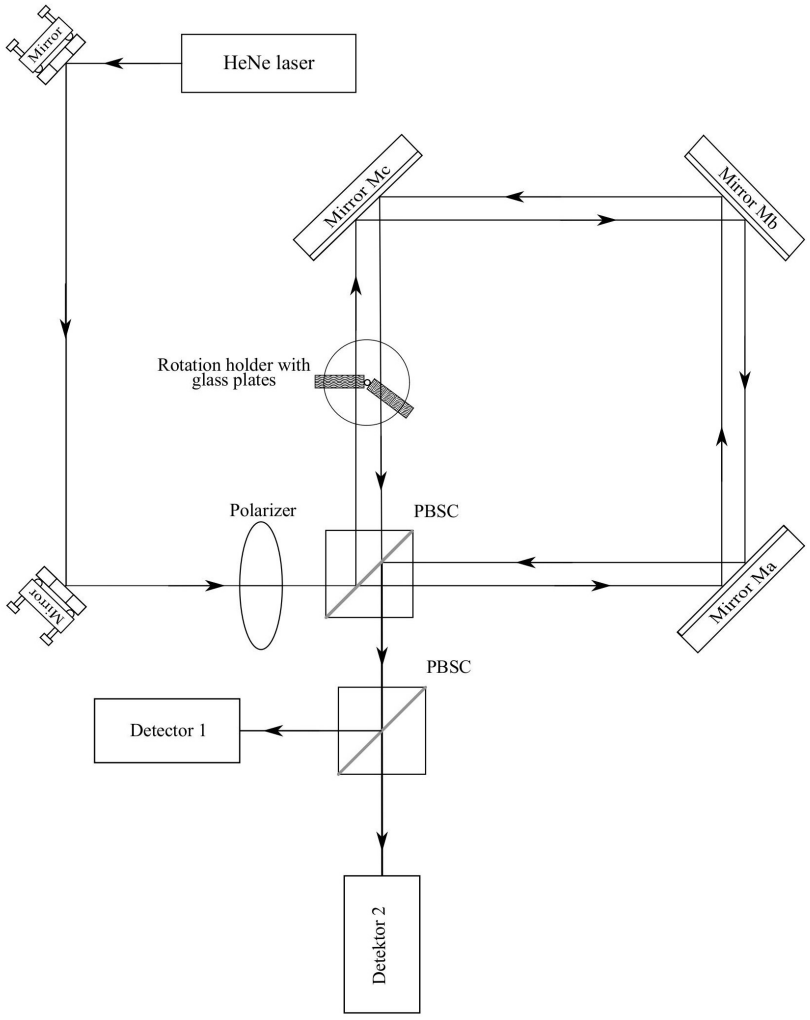

Figure 7: Schematic representation of the experimental setup after alignment.

3.2 Experimental Procedure

The procedure is divided into two parts: alignment and the actual experiment.

3.2.1 Alignment

At the start, the laser beam is coupled into the beam splitter (PBSC) using two mirrors. The mirrors Ma, Mb, and Mc are then aligned with respect to each other. Once all mirrors are correctly aligned, no interference pattern is visible after the PBSC, since the two overlapping beams are polarized perpendicular to each other. To separate the counter-propagating overlapping beams, the second input mirror is slightly shifted parallel to the interferometer, resulting in the beam path shown in Fig. 7. The rotatable glass

arrangement is then placed in one of the two beam paths. Finally, the signals from both detectors are processed into a differential signal and recorded. To prevent air pressure fluctuations, a Plexiglas cover is placed over the setup.

3.2.2 Measurements

The following measurements are performed sequentially on the interferometer:

(1.) To determine the contrast of the interferometer, initially only one detector is used. A fixed polarization angle is set at the polarizer, and the rotation mount with the two glass plates is rotated. The detector voltage is read in parallel using a multimeter, and three maxima and minima are recorded. The polarization angle is then increased by 15° each time until a total of 180° is reached, and for each angle, the minima and maxima are again determined by rotating the glass plates. Finally, the maximum contrast is calculated from the measured values, and the corresponding polarization angle is set at the polarizer.

(2.) To determine the refractive index of glass, both detectors are now operated using the differential voltage method. Both detectors are connected to the oscilloscope, and their difference is displayed. This method reduces measurement noise. The rotation mount for the two glass plates is rotated by a total of 10°, which changes the optical path length ($n \cdot L_{\text{geo.}}$) of both parallel beams. This results in interference, and the number of maxima occurring during the 10° rotation is recorded. This procedure is performed a total of 10 times.

(3.) The refractive index of air is determined by inserting a gas cuvette into one of the beam paths. The cuvette is first evacuated and then refilled with air. The number of intensity maxima in the interference pattern is recorded in steps of 50,0 mbar depending on the pressure in the cuvette. This measurement is repeated twice. The refractive index n under standard atmospheric conditions is then calculated from the measured values.

4 Analysis

In this section follows the analysis of the experiment. First the contrast of the interferometer is calculated with the measured data. Then the refractive indices of glass and air are computed. The calculations are done using *python* and the extension *uncertainties* [8] for the standard deviation. The extensions *matplotlib* [9] and *scipy* [10] are used for the plots and fits.

4.1 Polarization dependence of the contrast

For each polarization angle ϕ, the arithmetic mean and standard deviation of the three measurements of I_{max} and I_{min} are determined. Using Gaussian error propagation and

the definition

$$V(\phi) = \frac{I_{\max}(\phi) - I_{\min}(\phi)}{I_{\max}(\phi) + I_{\min}(\phi)}\,, \tag{16}$$

the contrast values $V(\phi)$ and their uncertainties $\Delta V(\phi)$ are obtained. The resulting data are shown with error bars in Fig. 8.

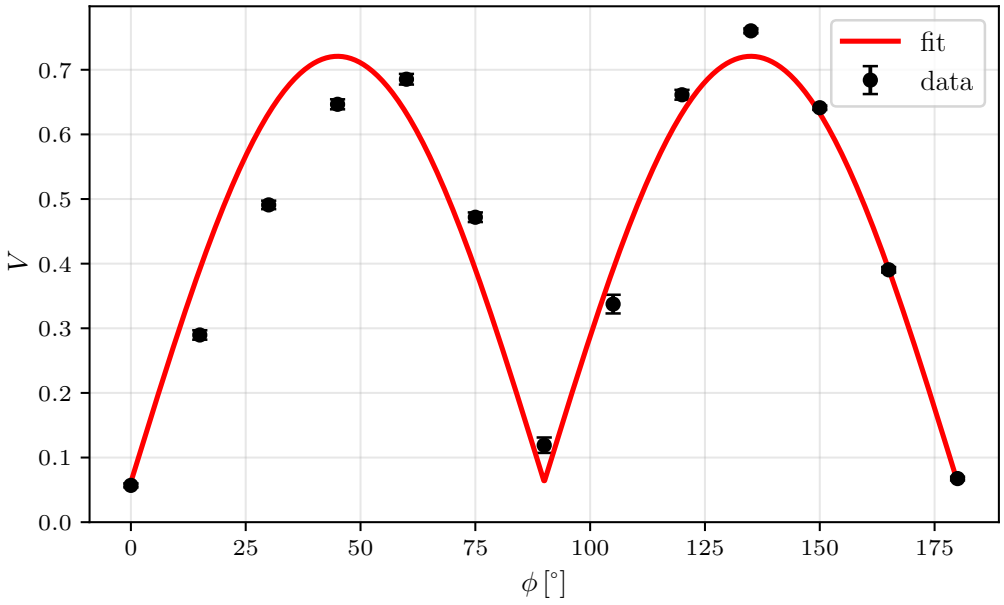

Figure 8: The plot shows the calculated contrast V as a function of the polarization angle ϕ together with a fit.

The angular dependence of the contrast is described by the model

$$V_{\text{model}}(\phi) = V_{\text{off}} + V_0 \left|\sin(2\phi)\right|\,, \tag{17}$$

where V_0 denotes the modulation amplitude and V_{off} a residual background contrast due to imperfections of the interferometer. The parameters V_0 and V_{off} are obtained from a weighted least-squares fit, in which each data point is weighted with $1/\Delta V(\phi_i)^2$. The uncertainties of the fitted parameters are derived from the covariance matrix of the weighted fit and correspond to the standard deviations of the fitted parameters. This yields

$$V_0 = 0.659 \pm 0.0032\,, \tag{18}$$

$$V_{\text{off}} = 0.062 \pm 0.0020\,. \tag{19}$$

The corresponding fit curve is shown in Fig. 8. The following measurements are performed at a polarization angle of $\phi = 135°$.

4.2 Refractive index of glass

For the measurment of the refractive index of glass a double glass is placed into the two beams. In the used setup the wavelength is $\lambda_{vac} = 632,99\text{nm}$, the initial rotation of the glass panes is $\Theta_0 = 10^\circ$ and the thickness of the glass panes is $d = 1\text{mm}$. By combining Equation 10 and Equation 12 the relation between the measured maxima and the refractive index is obtained:

$$n = \frac{1}{1 - \frac{\lambda_{vac} M}{2d\Theta_0 \Theta}}. \tag{20}$$

The measured maxima can be seen in Table 2. Assuming a counting uncertainty of one fringe for M and an angular precision of $\Delta\Theta \approx 1^\circ$ for the rotation angle, the resulting value for the refractive index of glass is

$$\bar{n}_{\text{glass}} = 1.4888 \pm 0.1032\,.$$

4.3 Refractive index of air

To determine the refractive index of air as a function of pressure, the number of interference maxima M_1, M_2 and M_3 passing through the centre of the interference pattern is recorded for each pressure value p between 50 and 996 mbar. The measured data are listed in Table 3. Using Equation 10 and Equation 13, the relation

$$\Delta n = \frac{M(p)\,\lambda_{\text{vac}}}{L} = n - 1 \tag{21}$$

is obtained between the measured pressure-dependent maxima $M(p)$, the laser wavelength $\lambda_{\text{vac}} = 632.996\,\text{nm}$, the length of the air cell $L = (100.0 \pm 0.1)\,\text{mm}$ and the refractive index of air n. The calculated values of Δn are listed in Table 3. At the same time, Equation 15 gives

$$\Delta n(p,T) = A \cdot \frac{3}{2R}\,\frac{p}{T}, \tag{22}$$

with the universal gas constant $R = 8.3144\,\text{J/(mol K)}$ and the molar refractivity A. The calculated values of Δn as a function of p are shown graphically in Figure 9.

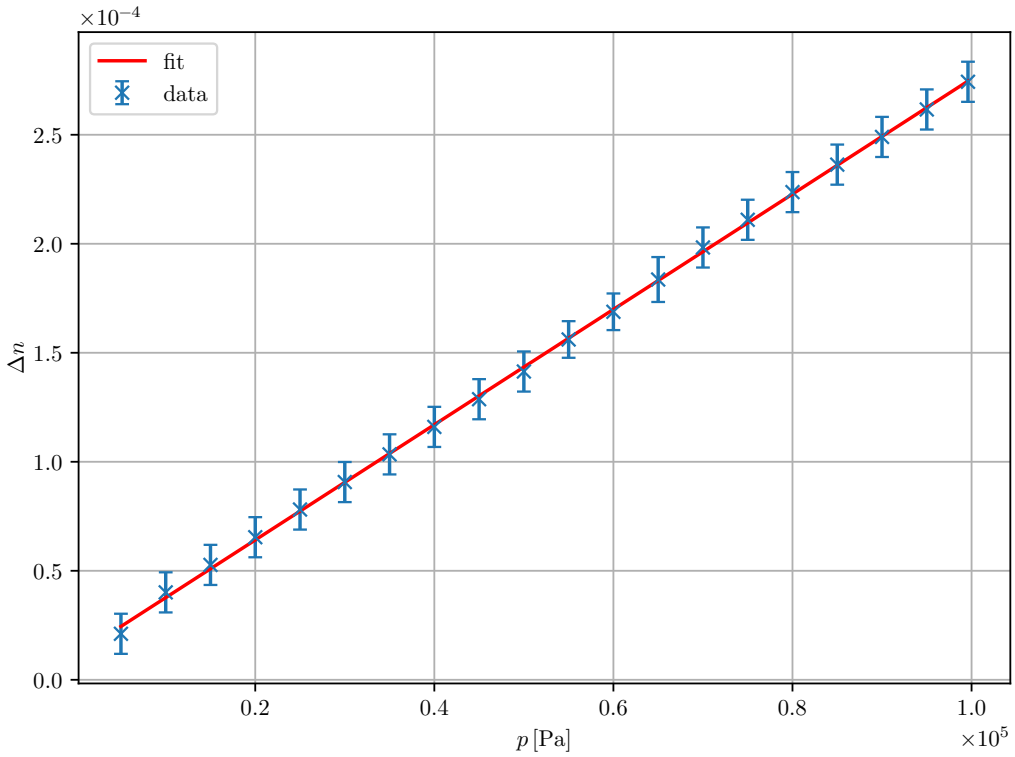

Figure 9: The plot shows the calculated difference in refractive index of air Δn in dependency of the pressure p and a fit.

In addition, a linear fit of the form

$$f(p) = c\,p + b \tag{23}$$

is performed, with the fit parameters

$$c = (2.64 \pm 0.01) \times 10^{-9}\,\mathrm{Pa}^{-1}\,, \tag{24}$$

$$b = (1.12 \pm 0.07) \times 10^{-5}\,. \tag{25}$$

The parameter c is related to the molar refractivity A via

$$c = A\,\frac{3}{2RT}\,. \tag{26}$$

Solving for A and inserting the measured temperature $T = 23.2^{\circ}\mathrm{C}$ yields

$$A = (4.34 \pm 0.02) \times 10^{-6}\,\mathrm{m}^3/\mathrm{mol}\,. \tag{27}$$

On the basis of these results, the following relation is obtained for the refractive index of air at arbitrary temperature T_0 and pressure p_0:

$$n_{\mathrm{air}}(T_0, p_0) = \underbrace{A\,\frac{3}{2R}\,\frac{p_0}{T_0} + b}_{\Delta n_{\mathrm{air}}(T_0, p_0)} + 1\,, \tag{28}$$

with $A = (4.34 \pm 0.02) \times 10^{-6}\,\mathrm{m}^3/\mathrm{mol}$ and $b = (1.12 \pm 0.07) \times 10^{-5}$. For the selected values $T_0 = 15.0^\circ\mathrm{C}$ and $p_0 = 1013.0\,\mathrm{hPa}$, insertion into Equation 28 gives

$$\Delta n_{\mathrm{air}}(T_0 = 15.0^\circ\mathrm{C},\, p_0 = 1013.0\,\mathrm{hPa}) = (0.0002867 \pm 0.0000014)\,, \tag{29}$$

$$n_{\mathrm{air}}(T_0 = 15.0^\circ\mathrm{C},\, p_0 = 1013.0\,\mathrm{hPa}) = 1.0002867 \pm 0.0000014\,. \tag{30}$$

Here, Δn denotes the actually measured quantity ($\Delta n = n - n_0$ with $n_0 = 1$ the refractive index of vacuum).

5 Discussion

The dependence of the polarization angle on the interferometer contrast showed overall good agreement between the measured data and the expected sinusoidal behaviour. The fit to the experimental data yields

$$V_0 = 0.659 \pm 0.0032\,, \tag{31}$$

$$V_{\mathrm{off}} = 0.062 \pm 0.0020\,, \tag{32}$$

so that a maximum visibility of $V_{\mathrm{max}} \approx 0.72$ is reached near $\phi \approx 45^\circ$ and 135°. An ideal interferometer would reach $V = 1$, therefore the obtained value indicates that the alignment is not perfect, but still sufficiently good to perform quantitative measurements. The non-zero offset V_{off} is consistent with the finite contrast observed at $\phi \approx 0^\circ$ and 90° and can be attributed to imperfections such as incomplete polarization purity, residual misalignment and stray reflections in the interferometer. The formal parameter uncertainties quoted above are derived from the covariance matrix of the weighted least–squares fit and thus reflect only the statistical component associated with the assigned visibility errors. The reduced chi-squared of the fit, however, is significantly larger than unity, indicating that the true experimental uncertainties are likely underestimated and that additional systematic variations are present. This should be kept in mind when interpreting the numerical values of V_0 and V_{off}.

The refractive index of glass is determined from the measured fringe shifts when rotating the glass plates in the interferometer arms. Using the known plate thickness, the rotation angles and an uncertainty estimate of one fringe for the counted maxima together with an angular precision of about 1°, the analysis yields

$$n_{\mathrm{glass,\,exp}} = 1.4888 \pm 0.1032\,. \tag{33}$$

Depending on the exact glass type, literature values for the refractive index at $\lambda \approx 633\,\mathrm{nm}$ are typically around $n_{\mathrm{glass,\,lit}} \approx 1.51$–$1.52$[11]. Taking $n_{\mathrm{glass,\,lit}} \approx 1.515$ as a representative value, the relative deviation of the experimental result is about $1.7\,\%$. Given the limited accuracy of the rotation angle, uncertainties in the effective plate thickness and possible non-ideal parallelism of the glass plates, as well as the unknown detailed glass composition, this level of agreement is satisfactory.

In the last part of the experiment, the refractive index of air is determined as a function of pressure. From the pressure-dependent number of observed fringes and the known

cell length, the quantity $\Delta n = n - 1$ is extracted and fitted with a linear function of pressure in accordance with the Lorentz–Lorenz relation. The fit parameters are used to determine the molar refractivity $A = (4.34 \pm 0.02) \times 10^{-6}\,\mathrm{m}^3/\mathrm{mol}$ and to extrapolate the refractive index of air to standard conditions ($T_0 = 15.0^\circ\mathrm{C}$, $p_0 = 1013.0\,\mathrm{hPa}$), resulting in

$$\Delta n_{\mathrm{air,\,exp}}(T_0, p_0) = (2.867 \pm 0.014) \times 10^{-4}\,, \tag{34}$$

$$n_{\mathrm{air,\,exp}}(T_0, p_0) = 1.0002867 \pm 0.0000014\,. \tag{35}$$

Typical literature values for dry air at comparable conditions and wavelength are around $n_{\mathrm{air,\,lit}} \approx 1.000276$ [12], i.e. $\Delta n_{\mathrm{air,\,lit}} \approx 2.76 \times 10^{-4}$. The relative deviation between the experimental and literature values of Δn is abaout 3.9 %, which is small in absolute terms but exceeds the purely statistical uncertainty from the fit. This suggests that additional systematic effects, which are not fully captured by the covariances of the fit parameters, play a role. Possible sources include uncertainties in the pressure calibration, deviations of the actual temperature from the assumed value, neglect of humidity in the Lorentz–Lorenz law, and residual misalignment or drift of the interferometer during the pressure scan.
Overall, the experiment succeeds in determining the refractive indices of glass and air with reasonable precision. The contrast measurement confirms that the interferometer alignment is adequate for quantitative work, even though the reduced chi-squared reveals that the visibility uncertainties are somewhat optimistic. The glass measurement is compatible with typical values for common optical glass within its relatively large error bar, and the air measurement reproduces the expected order of magnitude and pressure dependence of $n - 1$, with a small remaining deviation from literature values that can plausibly be attributed to systematic uncertainties and simplifying assumptions in the analysis.

6 Appendix

Table 1: Measurements for the polarisation angle dependency of the contrast K.

$\Phi/^\circ$	$I_{\mathrm{max},1}/\mathrm{V}$	$I_{\mathrm{min},1}/\mathrm{V}$	$I_{\mathrm{max},2}/\mathrm{V}$	$I_{\mathrm{min},2}/\mathrm{V}$	$I_{\mathrm{max},3}/\mathrm{V}$	$I_{\mathrm{min},3}/\mathrm{V}$
0	1,67	1,50	1,67	1,48	1,67	1,49
15	1,42	0,76	1,42	0,78	1,39	0,79
30	1,25	0,42	1,23	0,42	1,21	0,42
45	1,29	0,28	1,33	0,29	1,34	0,28
60	1,79	0,33	1,86	0,33	1,76	0,35
75	2,05	0,77	2,09	0,74	2,13	0,74
90	2,04	1,54	1,98	1,59	1,90	1,53
105	2,94	1,50	2,80	1,45	2,98	1,37
120	4,00	0,84	3,97	0,77	3,95	0,82
135	4,56	0,61	4,59	0,63	4,43	0,61
150	4,12	0,92	4,15	0,90	4,22	0,91
165	3,11	1,33	3,07	1,36	3,06	1,36
180	1,77	1,54	1,76	1,55	1,77	1,54

Table 2: Measurement of the maxima M passing the center of the interference spectrum in dependency of the tilt angle Θ of the glass planes.

$\Theta/^\circ$	M_1	M_2	M_3	M_4	M_5	M_6	M_7	M_8	M_9	M_{10}
10	31	32	32	32	32	31	31	31	32	32

Table 3: Measurement of the maxima M passing the center of the interference spectrum in dependency of the pressure p in the air chamber. In the last column are the calculated differences in refractive index Δn with the propagated standard deviations.

$p/mbar$	M_1	M_2	M_3	$\overline{\Delta n}/10^{-4}$
50	6	2	2	0.211 ± 0.092
100	9	5	5	0.401 ± 0.092
150	11	7	7	0.527 ± 0.092
200	13	9	9	0.654 ± 0.092
250	15	11	11	0.781 ± 0.092
300	17	13	13	0.907 ± 0.092
350	19	15	15	1.034 ± 0.092
400	21	17	17	1.160 ± 0.092
450	23	19	19	1.287 ± 0.092
500	25	21	21	1.414 ± 0.092
550	27	23	24	1.561 ± 0.084
600	29	25	26	1.688 ± 0.084
650	32	27	28	1.836 ± 0.103
700	34	30	30	1.983 ± 0.092
750	36	32	32	2.110 ± 0.092
800	38	34	34	2.237 ± 0.092
850	40	36	36	2.363 ± 0.092
900	42	38	38	2.490 ± 0.092
950	44	40	40	2.616 ± 0.092
996	46	42	42	2.743 ± 0.092

References

[1] Eugene Hecht. *Optik*. Berlin, Boston: De Gruyter Oldenbourg, 2023. ISBN: 9783111025599. DOI: doi:10.1515/9783111025599. URL: https://doi.org/10.1515/9783111025599.

[2] UHF PDA. *What are circularly polarized antennas and linearly polarized antennas in RFID?* https://www.uhfpda.com/news/what-are-circularly-polarized-antennas-and-linearly-polarized-antennas-in-rfid/. Accessed 2025-12-10. 2023.

[3] Leibniz Universität Hannover, PhysikPraktikum. *D14 Interferenz und Kohärenz*. Hannover: PhysikPraktikum. Verfügbar unter: https://www.praktikumphysik.uni-hannover.de/fileadmin/praktikumphysik/Versuche/HF/D-Optik/D14_HF.pdf. Mar. 2016.

[4] E. J. Post. "Sagnac Effect". In: *Reviews of Modern Physics* 39 (Apr. 1967), pp. 475–493. DOI: 10.1103/RevModPhys.39.475.

[5] Fulvio Ricci and Massimo Bassan. "The Sagnac Effect". In: *Experimental Gravitation*. Cham: Springer International Publishing, 2022, pp. 349–358. ISBN: 978-3-030-95596-0. DOI: 10.1007/978-3-030-95596-0_13. URL: https://doi.org/10.1007/978-3-030-95596-0_13.

[6] *Versuchsanleitung zu V46 "V64 Interferometry"*. TU Dortmund, Fakultät Physik. 2025.

[7] Helge Kragh. "The Lorenz–Lorentz Formula: Origin and Early History". In: *Substantia* 2.2 (Sept. 2018), pp. 7–18. DOI: 10.13128/Substantia-56. URL: https://riviste.fupress.net/index.php/subs/article/view/56.

[8] Eric O. Lebigot. *Uncertainties: a Python package for calculations with uncertainties*. Version 2.4.6.1. URL: http://pythonhosted.org/uncertainties/.

[9] John D. Hunter. "Matplotlib: A 2D Graphics Environment". Version 1.4.3. In: *Computing in Science & Engineering* 9.3 (2007), pp. 90–95. DOI: 10.1109/MCSE.2007.55. URL: http://matplotlib.org/. Current version 3.4.3, DOI: 10.5281/zenodo.5194481.

[10] Pauli Virtanen et al. "SciPy 1.0: Fundamental Algorithms for Scientific Computing in Python". In: *Nature Methods* 17 (2020), pp. 261–272. DOI: 10.1038/s41592-019-0686-2.

[11] SCHOTT AG. *SCHOTT N-BK7® Optical Glass – Data Sheet*. https://www.schott.com. Refractive index e.g. $n(632.8\,\mathrm{nm}) = 1.51509$. 2014.

[12] Philip E. Ciddor. "Refractive Index of Air: New Equations for the Visible and Near Infrared". In: *Applied Optics* 35.9 (1996), pp. 1566–1573. DOI: 10.1364/AO.35.001566.